T-ray Imaging: New Possibilities in the Far Infrared

Daniel M. Mittleman

Electrical and Computer Engineering Department, Rice University, MS-366, PO Box 1892, Houston TX 77251-1892

Abstract — **Since the initial demonstrations of T-ray imaging in 1995, there has been considerable progress in the development of this field. Many possible applications have been explored, and a commercial terahertz time-domain spectrometer is now operating in a manufacturing environment. In addition, several new imaging techniques which exploit the unique properties of the THz system have been developed. We describe one technique, which permits time-of-flight imaging with depth resolution well below the Rayleigh limit. We demonstrate the capability to resolve two reflecting surfaces separated by only a few percent of the coherence length of the THz radiation.**

I. INTRODUCTION

Within the last decade, there has been a revolution in THz technology, as a number of newly discovered or re-discovered generation and detection schemes have revitalized the field. These techniques, based on frequency conversion using non-linear optics [1,2,3,4,5], are often simpler, more reliable, and potentially much less expensive than the more traditional approaches. One of the first and most interesting of these non-linear optical techniques is *terahertz time-domain spectroscopy*, or THz-TDS [6]. The key components of a THz-TDS system are a femtosecond laser and a pair of specially designed transducers. By gating these transducers with ultrafast optical pulses, one can generate sub-picosecond bursts of THz radiation, and subsequently detect them with high signal-to-noise. These THz transients consist of only one or two cycles of the electromagnetic field, and they consequently span a very broad bandwidth. Bandwidths extending from ~100 GHz to 2 or 3 THz are routine, and more than 5 THz has been demonstrated [7]. Using free-space electro-optic sampling, bandwidths exceeding 40 THz have been reported [8]. Although the average intensity of the radiation is quite low, the high spatial coherence produces a brightness which exceeds that of conventional thermal sources. Finally, the gated detection provides a sensitivity comparable to the best bolometers, and requires no cryogenics or elaborate shielding.

In 1995, the first reports of imaging with THz-TDS generated a great deal of interest [9,10]. The value of a practical far-infrared imaging system has been recognized for some time, in a wide range of applications [11,12,13,14,15]. Because of the simplicity of the technique, THz-TDS has the potential to be the first THz imaging system which is portable, compact, and reliable enough for practical application in "real-world" environments. These advances have led to the development of the first commercial THz imaging spectrometer, shown in figure 1 [16]. This device is currently operating as an on-line monitoring system in a manufacturing environment.

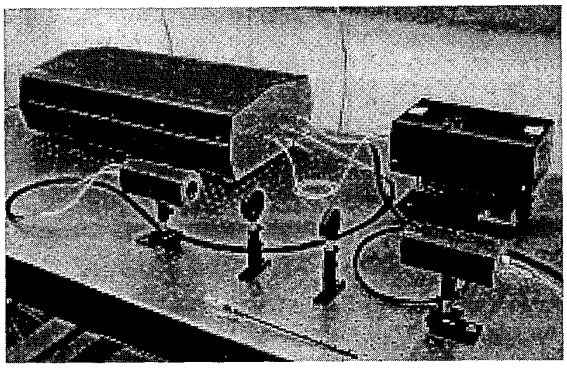

Fig. 1. A photo of the THz imaging spectrometer.

In this paper, we describe a few of the most interesting applications of THz 'T-ray' imaging. These include implementations in a reflection geometry, where the short duration of the THz pulses permits three-dimensional image reconstruction using time-of-flight techniques [17]. We then discuss a new imaging technique involving interferometry, which can be used to resolve two reflecting surfaces which are separated by much less than the coherence length of the radiation [18].

II. T-RAY IMAGING

In the most common implementation of T-ray imaging, pixels are acquired one at a time. The radiation emitted from a photoconducting antenna is broadband and spatially coherent, so it can be focused to a diffraction-limited spot. As a result, it is possible to form images by translating an object through the focal spot of the THz beam, and recording the transmitted or reflected waveform

0-7803-7239-5/02/$10.00 © 2002 IEEE

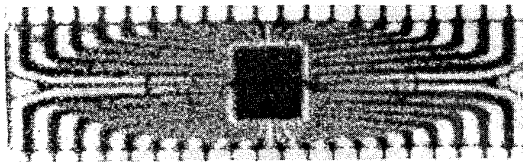

Fig. 2. THz image of an integrated circuit, showing the metal leads and the chip. The plastic packaging is nearly transparent.

as a function of the position of the object. The spatial resolution of a system of this type is determined by the spot size of the focused THz beam. This spot size is somewhat complicated, due to the broad bandwidth of the radiation, but a resolution below 0.5 mm is typical. Figure 2 shows an image of an integrated circuit which illustrates some of the capabilities of this system. Here, the transmitted THz energy is plotted as a gray scale, showing the decreased transmission through the metal leads and the silicon circuit. The plastic packaging is nearly transparent. It is worth noting that focal plane video-rate imaging has also been reported, although the laser power requirements are substantially higher [19].

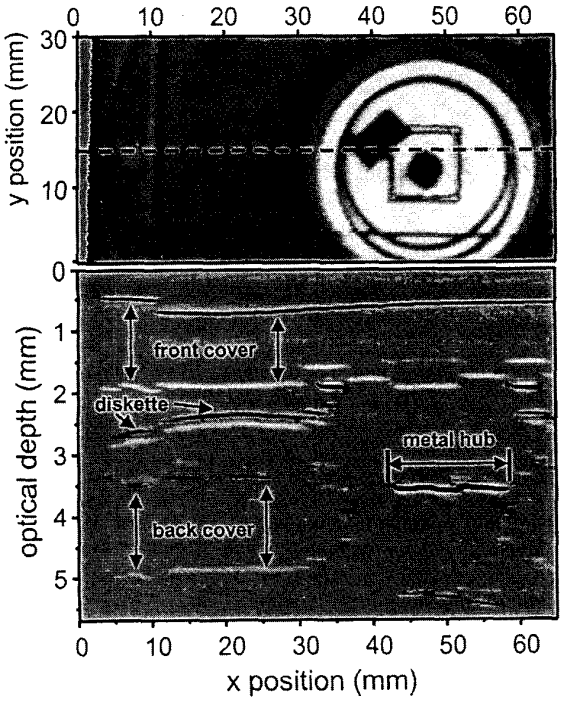

Fig. 3. The upper image shows the total reflected THz energy from the sample (a floppy disk). The lower image shows a tomographic slice through the sample, along the dashed line. Various buried interfaces can be discerned.

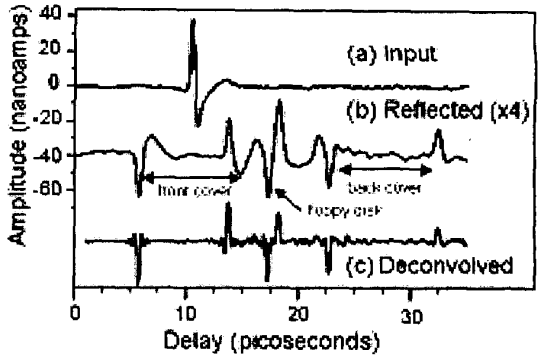

Fig. 4. (a) THz pulse incident on the sample (b) A typical reflected pulse train, showing a reflection in the time domain for each dielectric interface (c) Fourier deconvolution of the input pulse shape from the reflected pulse train. This permits resolution of the two surfaces of the thin recording medium.

Figure 3 shows a demonstration of an image formed in a reflection geometry. The upper panel shows the total reflected energy from the sample, a 3.5" floppy disk. The lower panel shows a slice through the object along the dashed line in the upper panel. Here, various buried dielectric interfaces can be discerned, each of which gives rise to a distinct reflected THz pulse. These include the front and rear surfaces of the two plastic covers, as well as the front and rear surface of the thin recording medium contained within.

Figure 4 shows a typical waveform reflected from this target, in which the various reflections can be distinguished. In this figure, the lower curve shows the Fourier deconvolution of the input pulse shape (a) from the reflected pulse train (b). This permits us to distinguish the two surfaces of the recording medium, even though in waveform (b) the corresponding two pulses are somewhat overlapped in time. This demonstrates the resolution limit of this time-of-flight technique – since the recording medium is only slightly thicker than $L_C/2$, where L_C is the coherence length of the THz radiation, it is only just possible to resolve the two surfaces. For these measurements, $L_C \sim 200$ μm.

II. Phase Shift Interferometry

The depth resolution illustrated above is a manifestation of a fundamental limit on any time-of-flight imaging technique, including both electromagnetic and acoustic imaging. It is equivalent to the Rayleigh criterion, well known in imaging optics. The ability to resolve two closely spaced reflecting surfaces is limited by the coherence length of the radiation in the intervening

medium, inversely proportional to its bandwidth. The only way to improve this depth resolution is to broaden the bandwidth of the source.

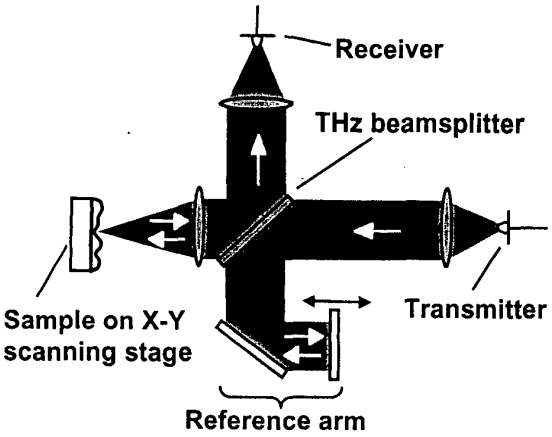

Fig. 5. A schematic of the setup for interferometric imaging.

Here, we describe a new imaging method which enables imaging well below the Rayleigh limit. A schematic of the setup is shown in figure 5. The THz pulse is injected into a Michaelson interferometer. The sample to be imaged is placed in one arm of the interferometer, at the focus of a lens. The two arms of the interferometer are adjusted to be of equal optical path length. In addition to providing the lateral resolution for imaging, the lens also imposes a phase shift of approximately π on the THz pulse, as a result of the Gouy phase shift. This phase shift is a purely topological effect, experienced by any wave passing through a focus [20]. As a result, the pulse reflecting from the sample is almost precisely out of phase with the pulse traversing the reference arm of the interferometer. The two pulses destructively interfere at the detector, and a very small signal is measured. However, if the sample modifies either the amplitude or phase of the pulse, then this destructive interference is disrupted and a large signal is measured.

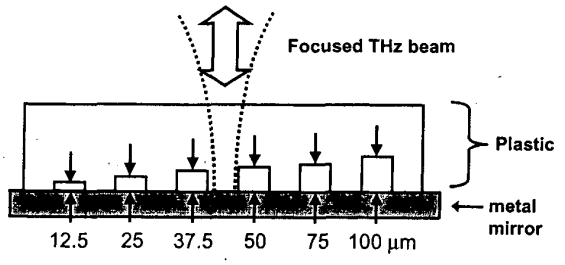

Fig. 6. A schematic of the sample fabricated to test the resolution of the imaging system. It consists of a layer of teflon with a series of calibrated grooves machined into one side. This is then sandwiched against a metal reflector, to form a series of air gaps of known width. The widths are shown. The sample is placed in the focus of the THz beam, as shown.

The use of interferometry affords several advantages in the detection of subtle features in a sample. First, the fractional change in peak-to-peak amplitude is much larger with interferometry. This provides both an increased contrast in the imaging of dielectric discontinuities, and an enhanced sensitivity for the detection of sub-coherence-length layers, as shown below. Interferometry also provides a background-free method for waveform acquisition, which naturally eliminates common-mode noise arising from laser fluctuations or other external perturbations.

To demonstrate the ability to image below the Rayleigh limit, we have constructed several model samples containing thin, well-controlled features. Figure 6 shows a schematic of one Teflon-metal model, with air gaps between the two pieces ranging from 12.5 μm to 100 μm in width. This model is positioned so that the metal-plastic interface is located at the focus of the imaging lens in the sample arm. We image a line scan across this sample, and compare the results with and without the interferometric cancellation. In figure 7, we show the percent change in the peak-to-peak amplitude of the measured waveform relative to a waveform measured at a position on the sample containing no air gap. The dashed curve shows the

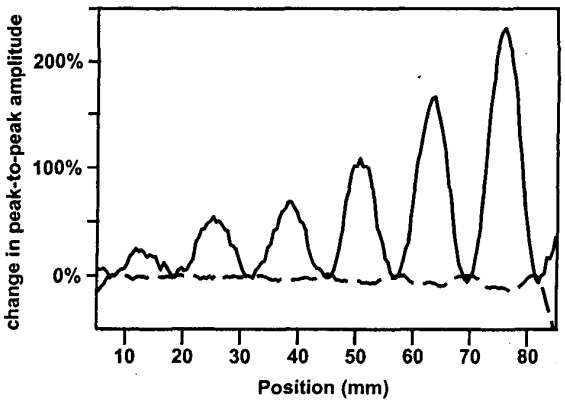

Fig. 7. Line scan images of the sample shown in figure 9. These show the change in peak-to-peak amplitude of the waveform, relative to a waveform measured at a position where there is no air gap, as a function of position along a line across the sample, slicing through the six air gaps. The solid curve shows the result when interferometry is employed, while the dashed curve shows the result without interferometry. The coherence length of the pulse for these measurements was ~315 μm.

result without interferometry, while the solid curve shows the much more dramatic modulation that results when interferometry is employed. As a result, it is possible to easily detect the smallest air gap using the interference effect. This 12.5 μm gap is roughly 25 times thinner than the coherence length of the pulses used to collect this data.

In conclusion, we have demonstrated a new imaging technique which relies on the Gouy phase shift to provide a nearly background-free signal. This results in a dramatic enhancement in the depth resolution and the sensitivity to small or subtle features in a sample. We note that the transverse resolution in these measurements is quite poor, owing to the relatively low bandwidth of the THz source used. Even so, phase shift interferometry permits us to image with a depth resolution that is more than 100 times better than the transverse resolution. Finally, it is worth emphasizing that this technique is quite general, in the sense that the Gouy phase is a purely geometrical effect applicable to any focused electromagnetic wave. Similar enhancement factors can be expected when this technique is applied in other spectral regimes.

ACKNOWLEDGEMENT

The phase shift interferometry experiments have been performed by Jon Johnson. We also acknowledge the participation of Rune Jacobsen, Stefan Hunsche, Luc Boivin, and Martin Nuss in THz imaging experiments. This work has been funded in part by the National Science Foundation and the Environmental Protection Agency.

REFERENCES

[1] A. Nahata, D. H. Auston, and T. F. Heinz, "Coherent detection of freely propagating terahertz radiation by electro-optic sampling," *Appl. Phys. Lett.*, **68**, 150 (1996).

[2] K. Kawase, M. Sato, T. Taniuchi, and H. Ito, "Coherent tunable THz-wave generation from LiNbO3 with monolithic grating coupler," *Appl. Phys. Lett.*, **68**, 2483 (1996).

[3] S. Verghese, K. A. McIntosh, and E. R. Brown, "Highly tunable fiber-coupled photomixers with coherent terahertz output power," *IEEE Trans. Microwave Th. Tech.*, **45**, 1301 (1997).

[4] M. C. Nuss, P. C. M. Planken, I. Brener, H. G. Roskos, M. S. C. Luo, and S. L. Chuang, "Terahertz electromagnetic radiation from quantum wells," *Appl. Phys. B*, **58**, 249 (1994).

[5] L. Xu, X.-C. Zhang, and D. H. Auston, "Terahertz beam generation by femtosecond optical pulses in electro-optic materials," *Appl. Phys. Lett.*, **61**, 1784 (1992).

[6] P. R. Smith, D. H. Auston, and M. C. Nuss, "Subpicosecond photoconducting dipole antennas," *IEEE J. Quant. Elec.*, **24**, 255 (1988).

[7] S. E. Ralph, S. Perkowitz, N. Katzenellenbogen, and D. Grischkowsky, "Terahertz spectroscopy of optically thick multilayered semiconductor structures," *J. Opt. Soc. Am. B*, **11**, 2528 (1994).

[8] R. Huber, A. Brodschelm, F. Tauser, and A. Leitenstorfer, "Generation and field-resolved detection of femtosecond electromagnetic pulses tunable up to 41 THz," *Appl. Phys. Lett.*, **76**, 3191 (2000).

[9] B. B. Hu and M. C. Nuss, "Imaging with terahertz waves," *Opt. Lett.*, **20**, 1716 (1995).

[10] D. Mittleman, R. H. Jacobsen, and M. C. Nuss, "T-ray imaging," *IEEE J. Sel. Top. Quant. Elec.*, **2**, 679 (1996).

[11] T. S. Hartwick, D. T. Hodges, D. H. Barker, and F. B. Foote, "Far infrared imagery," *Appl. Opt.*, **15**, 1919 (1976).

[12] A. J. Cantor, P. K. Cheo, M. C. Foster, and L. A. Newman, "Application of submillimeter wave lasers to high voltage cable inspection," *IEEE J. Quant. Elec.*, **17**, 477 (1981).

[13] N. Gopalsami, S. Bakhtiari, S. L. Dieckman, A. C. Raptis, and M. J. Lepper, "Millimeter-wave imaging for nondestructive evaluation of materials," *Mater. Eval.*, **52**, 412 (1994).

[14] N. C. Currie, F. J. Demma, D. D. Ferris Jr., R. W. McMillan, V. C. Vannicola, and M. C. Wicks, "Survey of state-of-the-art technology in remote concealed weapon detection," *Proc. SPIE*, **2567**, 124 (1995).

[15] C. M. Ciesla, D. D. Arnone, A. Corchia, D. Crawley, C. Longbottom, E. H. Linfield, and M. Pepper, "Biomedical applications of terahertz pulse imaging," *Proc. SPIE*, **3934**, 73 (2000).

[16] J. V. Rudd, D. Zimdars, and M. Warmuth, "Compact fiber-pigtailed terahertz imaging system," *Proc. SPIE*, **3934**, 27 (2000).

[17] D. M. Mittleman, S. Hunsche, L. Boivin, and M. C. Nuss, "T-ray tomography," *Opt. Lett.*, **22**, 904 (1997).

[18] J. L. Johnson, T. D. Dorney, and D. M. Mittleman, "Enhanced depth resolution in terahertz imaging using phase-shift interferometry," *Appl. Phys. Lett.*, **78**, 835 (2001)

[19] Z. Jiang and X.-C. Zhang, "Terahertz imaging via electrooptic effect," *IEEE Trans. Microwave Th. Tech.*, **47**, 2644 (1999).

[20] A. B. Ruffin, J. V. Rudd, J. F. Whitaker, S. Feng, and H. G. Winful, "Direct observation of the Gouy phase shift with single-cycle terahertz pulses," *Phy. Rev. Lett.* **83**, 3410 (1999).